

The drying of liquid droplets

Zechao Jiang(姜泽超), Xiuyuan Yang(杨修远), Mengmeng Wu(吴萌萌), Xingkun Man(满兴坤)

Citation: Chin. Phys. B . 2020, 29(9): 096803 . **doi:** 10.1088/1674-1056/ab8ac7
Journal homepage: http://cpb.iphy.ac.cn; http://iopscience.iop.org/cpb

What follows is a list of articles you may be interested in

Growth and aggregation of Cu nanocrystals on ionic liquid surfaces

Jia-Wei Shen(沈佳伟), Xun-Heng Ye(叶迅亨), Zhi-Long Bao(鲍志龙), Lu Li(李璐), Bo Yang(杨波), Xiang-Ming Tao(陶向明), Gao-Xiang Ye(叶高翔)

Chin. Phys. B . 2020, 29(6): 066801 . **doi:** 10.1088/1674-1056/ab8896

Charge trapping memory device based on the Ga_2O_3 films as trapping and blocking layer

Bing Bai(白冰), Hong Wang(王宏), Yan Li(李岩), Yunxia Hao(郝云霞), Bo Zhang(张博), Boping Wang(王博平), Zihang Wang(王子航), Hongqi Yang(杨红旗), Qihang Gao(高启航), Chao Lü(吕超), Qingshun Zhang(张庆顺), Xiaobing Yan(闫小兵)

Chin. Phys. B . 2019, 28(10): 106802 . **doi:** 10.1088/1674-1056/ab3e62

Effect of deposited temperatures of the buffer layer on the band offset of CZTS/In_2S_3 heterostructure and its solar cell performance

Jinling Yu(俞金玲), Zhongming Zheng(郑重明), Limei Dong(董丽美), Shuying Cheng(程树英), Yunfeng Lai(赖云锋), Qiao Zheng(郑巧), Haifang Zhou(周海芳), Hongjie Jia(贾宏杰), Hong Zhang(张红)

Chin. Phys. B . 2017, 26(4): 046802 . **doi:** 10.1088/1674-1056/26/4/046802

Skin formation in drying a film of soft matter solutions: Application of solute based Lagrangian scheme

Ling Luo(罗凌), Fanlong Meng(孟凡龙), Junying Zhang(张俊英), Masao Doi

Chin. Phys. B . 2016, 25(7): 076801 . **doi:** 10.1088/1674-1056/25/7/076801

Optical and electrical characterizations of nanoparticle Cu_2S thin films

M. Saadeldin, H. S. Soliman, H. A. M. Ali, K. Sawaby

Chin. Phys. B . 2014, 23(4): 046803 . **doi:** 10.1088/1674-1056/23/4/046803

The drying of liquid droplets*

Zechao Jiang(姜泽超)[1,2], Xiuyuan Yang(杨修远)[1,2], Mengmeng Wu(吴萌萌)[1,2], and Xingkun Man(满兴坤)[1,2,†]

[1] *Center of Soft Matter Physics and Its Applications, Beihang University, Beijing* 100191, *China*
[2] *School of Physics, Beihang University, Beijing* 100191, *China*

(Received 12 March 2020; revised manuscript received 13 April 2020; accepted manuscript online 18 April 2020)

The drying of liquid droplets is a common phenomenon in daily life, and has long attracted special interest in scientific research. We propose a simple model to quantify the shape evolution of drying droplets. The model takes into account the friction constant between the contact line (CL) and the substrate, the capillary forces, and the evaporation rate. Two typical evaporation processes observed in experiments, i.e., the constant contact radius (CCR) and the constant contact angle (CCA), are demonstrated by the model. Moreover, the simple model shows complicated evaporation dynamics, for example, the CL first spreads and then recedes during evaporation. Analytical models of no evaporation, CCR, and CCA cases are given, respectively. The scaling law of the CL or the contact angle as a function of time obtained by analytical model is consistent with the full numerical model, and they are all subjected to experimental tests. The general model facilitates a quantitative understanding of the physical mechanism underlying the drying of liquid droplets.

Keywords: evaporation, droplets, Onsager variational principle, contact line motion

PACS: 68.03.Fg, 45.10.Db, 82.20.Wt **DOI:** 10.1088/1674-1056/ab8ac7

1. Introduction

The drying of droplets of particle suspensions and polymer solutions on substrates can produce rich deposition patterns,[1,2] including coffee-ring,[3,4] mountainlike,[5–7] volcanolike,[8,9] and multi-ring patterns.[10] The drying of liquid droplets is a common phenomenon in daily life, and has practical applications such as inkjet printing,[11] pesticide spraying,[12] semiconductor industry production,[13] etc. The dynamics of droplet evaporation therefore has long been of special interest in scientific research.

Evaporating droplets show complex shape evolution modes that the contact radius can increase or decrease with time under different conditions.[14–21] In 1977, Picknett and Bexon[14] reported on the mass and profile evolution of a slowly evaporating liquid (methyl acetoacetate) drop on a polytetrafluoroethylene (PTFE) surface in still air. They distinguished three evaporation modes: constant contact radius (CCR) mode, constant contact angle (CCA) mode, and mixed mode which changes from one to the other at some point or both contact angle and contact radius change simultaneously. Bourgès-Monnier and Shanahan[15] showed that the contact angle of water and n-decane droplets remain constant in the saturated vapor atmosphere conditions, and diminishing the atmospheric vapor content can lead to marked reductions of contact angle during the drying process. While in open air conditions, the evaporation process has been split into four stages. Erbil[16] *et al.* studied the CCA evaporation mode through the evaporation of n-butanol, toluene, n-nonane, and n-octane drops on a PTFE surface. They found that the decrease of the contact area of these drops is linear with time. On the other hand, Kim *et al.*[17] reported that the receding angle and the Marangoni instability are two main physical factors influencing the transition of evaporation mode during the drying process of water droplets, which result from the concentration gradient of contaminants in water.

In view of the experimental studies, there are a few theoretical and simulation works addressing the shape evolution of drying droplets. Wang *et al.*[19] studied the contact line dynamics of nanodroplets on different chemically inhomogeneous surfaces using molecular dynamics method. For the evaporation of a nano-droplet on the surface with large characteristic width of the inhomogeneity, the contact line pinned on the substrate at the initial stage of the evaporation and exhibited the CCR mode. While on the surfaces with smaller characteristic width, only the CCA and mixed modes can be found during the evaporation. Liu and Zhang[20] investigated the evaporation dynamics of nanodroplets sitting on smooth and rough substrates using the kinetic lattice density functional theory (KLDFT). They reported that on smooth substrates, the droplets generally evaporate in the CCA mode, while on rough substrates, the droplets evaporate in the CCR mode or the mixed mode.

The deposition pattern of drying droplets has been widely studied experimentally and theoretically over the past three decades. The seminal work by Deegan *et al.*[22] established

*Project supported by the National Natural Science Foundation of China (Grant No. 21822302), the joint NSFC-ISF Research Program, China (Grant No. 21961142020), the Fundamental Research Funds for the Central Universities, China, and the National College Students' Innovative and Entrepreneurial Training Plan Program, China (Grant No. 201910006142).

†Corresponding author. E-mail: manxk@buaa.edu.cn

© 2020 Chinese Physical Society and IOP Publishing Ltd

the basic principles that govern the deposition pattern, which is mainly based on the evaporation-induced fluid flow inside the droplet and the pinning of droplet contact line (CL). Hu and Larson[23,24] carefully compared the results from full numerical simulations with the experiments, and pointed out the importance of the Marangoni effect in the final deposition pattern. Freed-Brown[25] proposed a simple model assuming that the contact line moves freely so that the contact angle remains constant. This model explained the formation mechanism of the mountainlike deposition pattern. Multi-rings have been explained experimentally[26] and theoretically[27] by the stick-slip motion of the contact line. Recently, Thampi[28] performed an exhaustive numerical study of the contact line evolution during droplet evaporation. They showed that the motion of droplet contact line is mainly parameterized by the substrate wettability. Previous theoretical models were written in the form of nonlinear partial differential equations and required numerical simulation to see the outcome of the model. Moreover, these models are usually for one special situation, lacking the generality in understanding the deposition pattern formation mechanism.

In recent years, we have proposed an Onsager variational principle theory to study the drying of liquid droplets by assuming the contact angle being small and the liquid/vapor interface having a parabolic form. In fact, the contact angle of droplets can be large, and a spherical shape of the liquid/vapor interface is more common in nature. So in this article, we propose a more general model without the assumption of small contact angle. It is worth pointing out that the model automatically goes back to the previous model when the contact angle is small.

Using Onsager variational principle theory, we derive a general shape evolution equation for drying droplets. This model reveals three main droplet shape evolution modes observed in experiments: the constant contact angle evaporation process, the constant contact radius, and a mixture of the two modes. Analytical expressions of the contact angle and the contact radius as a function of evaporation time are given. The simple model also recovers the famous Tanner's law.

2. Model and theory

2.1. Droplet shape evolution equation

Onsager variational principle[29–31] was proposed by Onsager in his celebrated paper[32,33] about the reciprocal relation. This theory provides an applicable method to study the dynamic process of various nonlinear and non-equilibrium phenomena of soft matter, such as phase separation,[34] gel dynamics,[35] colloidal dynamics, and molecular modeling for viscoelasticity. One important aspect of this theory is that Onsager variational principle can facilitate establishing nonlinear time evolution equations. In fact, for isothermal process, this principle is also referred to as the minimum energy dissipation principle in hydrodynamics.

We assume that the liquid/vapor interface of the droplet has a spherical shape. This assumption allows the calculations for droplet on both hydrophilic and hydrophobic substrates. It indicates that the droplet contact angle can vary from 0 to $\pi/2$ in the following calculations. The schematic in Fig. 1(b) shows that one droplet is placed on a substrate, and has cylindrical symmetry. The droplet has the height at the center $H(t)$, contact radius $r(t)$, contact angle $\theta(t)$, and volume $V(t)$, while $R(t)$ is the radius of the spherical crown of liquid/vapor interface. We define α as the circumference angle of one point at the liquid/vapor interface. With all these definitions, we have the following relations:

$$\begin{aligned} x &= R\sin\alpha, \\ r &= R\sin\theta, \\ H &= R(1-\cos\theta), \\ h &= R(\cos\alpha-\cos\theta), \\ V &= \frac{1}{3}\pi R^3(1-\cos\theta)^2(2+\cos\theta). \end{aligned} \tag{1}$$

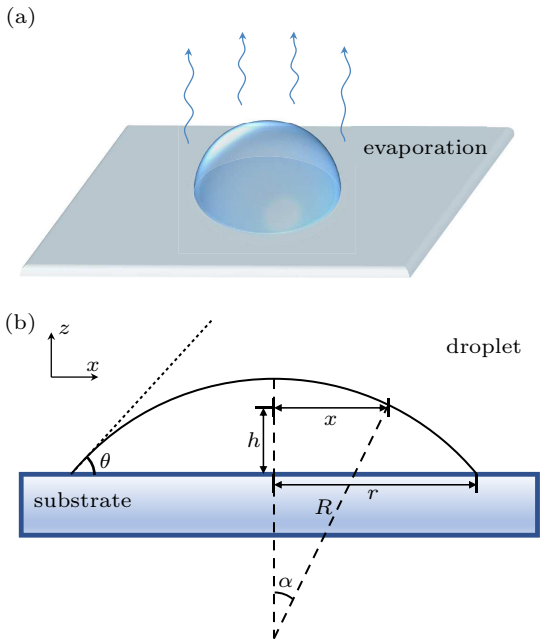


Fig. 1. Schematic of a sessile droplet drying on a substrate. Panels (a) and (b) are the top and the side views of the droplet, respectively. Relevant parameters are the radius of the contact line r, the radius of the spherical crown R, the contact angle θ, the height of the droplet h at position x.

The volume $V(t)$ of the droplet decreases with time due to solvent evaporation. The evaporation rate of a droplet is determined by the diffusion of solvent molecules in the gas phase, and can be analyzed theoretically. When there is no air flow near the liquid surface, $\dot{V}(t)$ can be obtained by solving the diffusion equation of solvent vapor in air. It has been shown that $\dot{V}(t)$ is proportional to the base radius of the droplet,[36,37]

and is weakly dependent on the contact angle. Therefore, we ignore the contact angle dependence, and assume that

$$\dot{V}(t) = \dot{V}_0 \frac{r(t)}{r_0} = \dot{V}_0 \frac{R(t)\sin\theta}{R_0 \sin\theta_0}, \tag{2}$$

where $\dot{V}_0$ (≤ 0) and r_0 denote the initial values of $\dot{V}(t)$ and $r(t)$, respectively. $\dot{V}_0$ is expressed in terms of the diffusion constant of the solvent molecules in the gas phase, the solvent vapor pressure near and far from the droplet, and the temperature. The evaporation rate (the volume of solvent evaporated per unit time per unit surface area) is given by

$$J(t) = -\frac{\dot{V}(t)}{\pi r^2(t)} = -\frac{\dot{V}_0}{\pi r_0 r(t)}. \tag{3}$$

In order to obtain the evolution model of droplets during evaporation, we calculate the evolution equation $\dot{R}(t)$, by using Onsager variational principle. Then, we can obtain the droplet shape evolution equation $\dot{r}$ and $\dot{\theta}$ from $\dot{R}$. We take R and θ as the slow variables. The theory starts from the Rayleighian that comprises two parts: the time derivative of the free energy, $\dot{F}$ and the energy dissipation function Φ

$$\Re = \Phi + \dot{F}. \tag{4}$$

The droplet size is assumed to be less than the capillary length, then the free energy F is written as a sum of the interfacial energies

$$\begin{aligned} F &= (\gamma_{\rm LS} - \gamma_{\rm SV})\pi r^2 + \gamma_{\rm LV} \cdot \int_0^\theta 2\pi x R \mathrm{d}\alpha \\ &= \pi R^2 \gamma_{\rm LV} \left[-\sin^2\theta\cos\theta_{\rm e} + 2(1-\cos\theta) \right], \end{aligned} \tag{5}$$

where $\gamma_{\rm LV}$, $\gamma_{\rm LS}$, and $\gamma_{\rm SV}$ are the surface tensions at liquid/vapor, liquid/substrate, and substrate/vapor, respectively. The equilibrium contact angle is given by the Young's equation

$$\cos\theta_{\rm e} = \frac{\gamma_{\rm SV} - \gamma_{\rm LS}}{\gamma_{\rm LV}}. \tag{6}$$

Then, the time derivative of such a free energy is

$$\begin{aligned} \dot{F} &= 2\gamma_{\rm LV}\pi R \left[\dot{R}(2 - 2\cos\theta - \sin^2\theta\cos\theta_{\rm e}) \right. \\ &\quad \left. + R\sin\theta\dot{\theta}(1 - \cos\theta\cos\theta_{\rm e}) \right]. \end{aligned} \tag{7}$$

We calculate the energy dissipation function, Φ, by taking the lubrication approximation. Let $v(x,t)$ be the height-averaged fluid velocity at position x and time t. The energy dissipation function Φ is written as

$$\Phi = \frac{1}{2}\int_0^r 2\pi x \frac{3\eta}{h} v^2 \mathrm{d}x + \pi\xi_{\rm cl} r \dot{r}^2. \tag{8}$$

The dissipation function has two parts. The first term is the usual hydrodynamic energy dissipation in the lubrication approximation, while the second term is the energy dissipation from the motion of the contact line over the substrate.[38] The parameter $\xi_{\rm cl}$ is a phenomenological parameter of the mobility of the contact line: the droplet would be pinned on the substrate when $\xi_{\rm cl}$ is large enough, and can move freely when $\xi_{\rm cl} = 0$.

Experiments have shown that $\xi_{\rm cl}$ originates from the substrate wetting properties, substrate defects, and surface-active solutes. Since not much is known about the quantitative relation between $\xi_{\rm cl}$ and all these factors, in the following, we define a dimensionless parameter $k_{\rm cl} = \xi_{\rm cl}/\eta$ and proceed to make a simple assumption that $\xi_{\rm cl}$ is a constant phenomenological parameter. We define such a $k_{\rm cl}$ as the effective friction constant between the contact line and the substrate to indicate the mobility of the contact line. For weak contact angle hysteresis (CAH) substrate, the CL mobility is strong, corresponding to small values of $k_{\rm cl}$. On the other hand, for strong CAH substrate, the CL is pinned. We therefore set a large value of $k_{\rm cl}$.

The height-averaged fluid velocity at position x and time t, $v(x,t)$, is obtained by solving the mass conservation equation

$$\dot{h} = -\frac{1}{x}\frac{\partial}{\partial x}(xvh) - J. \tag{9}$$

With Eqs. (1), (3) , and (9), We obtain the simple expression of $v(x,t)$

$$v(x,t) = \dot{R}\frac{(\cos\alpha - 1)(\cos\alpha\cos\theta + \cos\alpha + \cos\theta)}{\sin\alpha(1+\cos\theta)}. \tag{10}$$

Then, the energy dissipation function Φ becomes

$$\begin{aligned} \Phi &= 3\pi\eta R\dot{R}^2 C_1(\theta) + \pi\xi_{\rm cl} R\sin^3\theta\dot{R}^2 + \pi\xi_{\rm cl}R^3\sin\theta\cos^2\theta\dot{\theta}^2 \\ &\quad + 2\pi\xi_{\rm cl}R^2\sin^2\theta\cos\theta\dot{R}\dot{\theta}, \end{aligned} \tag{11}$$

where

$$\begin{aligned} C_1(\theta) &= \frac{11}{6}\cos^3\theta - \cos^2\theta - \frac{9}{2}\cos\theta + \frac{23}{3} \\ &\quad - \frac{7}{1+\cos\theta} - \frac{2}{(1+\cos\theta)^2} \\ &\quad + \frac{\cos^3\theta(1-\cos\theta)(2+\cos\theta)^2}{(1+\cos\theta)^3}\ln\frac{1-\cos\theta}{\varepsilon} \\ &\quad + \frac{2}{(1+\cos\theta)^3}\ln\frac{2}{1+\cos\theta}, \end{aligned} \tag{12}$$

and ε is the molecular cutoff length, which is introduced to remove the divergence in the energy dissipation at the contact line.

The Onsager principle states that $\dot{R}$ is determined by the condition

$$\begin{aligned} \frac{\partial(\Phi + \dot{F})}{\partial\dot{R}} &= 6\pi\eta R\dot{R}C_1(\theta) + 2\pi\xi_{\rm cl}R\dot{R}C_2(\theta) \\ &\quad + 2\xi_{\rm cl}\frac{\dot{V}}{R}C_3(\theta) + 2\pi\gamma_{\rm LV}RC_4(\theta) \\ &= 0, \end{aligned} \tag{13}$$

where

$$C_2(\theta)=\frac{(1-\cos\theta)^2}{\sin\theta(1+\cos\theta)^2},\quad C_3(\theta)=\frac{\cos\theta}{\sin\theta(1+\cos\theta)^2},$$
$$C_4(\theta)=\frac{1-\cos\theta}{1+\cos\theta}(\cos\theta-\cos\theta_e).$$

To simplify the equations, we define the evaporation time τ_{ev} and relaxation time τ_{re} by

$$\tau_{ev}=-\frac{V_0}{\dot{V}_0},\quad \tau_{re}=\frac{\eta r_0}{\gamma_{LV}}, \tag{14}$$

where τ_{ev} represents the characteristic time taken by the initial droplet to dry up, and τ_{re} represents the characteristic time taken by the initial droplet to reach its equilibrium state. k_{ev} is defined by

$$k_{ev}=\frac{\tau_{re}}{\tau_{ev}}, \tag{15}$$

which represents the evaporation rate. The evaporation rate increases when k_{ev} increases.[37]

2.2. Comparison with convention hydrodynamics theory

When there is no evaporation, the liquid volume does not change, $\dot{V}=0$. Then we obtain the function

$$\begin{cases}\dfrac{\partial(\Phi+\dot{F})}{\partial\dot{R}}=0,\\ \dot{V}=0.\end{cases} \tag{16}$$

The evolution of rescaled r and θ becomes

$$\begin{cases}\tau_{re}\dot{\tilde{r}}=-\dfrac{(1-\cos\theta)^2}{3C_1(\theta)\sin\theta(1+\cos\theta)^2}(\cos\theta-\cos\theta_e),\\ \tau_{re}\dot{\theta}=\dfrac{(1-\cos\theta)^2(2+\cos\theta)}{3C_1(\theta)(1+\cos\theta)^2\tilde{r}}(\cos\theta-\cos\theta_e),\end{cases} \tag{17}$$

where $\tilde{r}=r/r_0$, and r_0 is the initial contact radius of the droplet.

This is a full model of the droplet shape evolution when there is no evaporation. We show that the famous Tanner's law can be naturally obtained from the model. According to the condition of Tanner's law,[39] we assume that the droplet is placed on a superwetting substrate with a small initial contact angle.

Then, the evolution equation of $\tilde{r}$ becomes

$$\tau_{re}\dot{\tilde{r}}\approx k_1\theta^{-3}=k_2\tilde{r}^{-9}, \tag{18}$$

which has the same power law of $\tilde{r}$ as a function of time as the Tanner's law.

Figure 2 shows the evolution of the droplet contact line for various values of initial contact angle θ_0. When θ_0 is not equal to its equilibrium value, the droplet will relax to its equilibrium shape. The fitting slopes of three log–log curves of $\tilde{r}(t)$ are all close to 0.1, which is good verification of Tanner's law. The spreading of the contact line is governed by the capillary and viscous forces. The capillary force is raised by the difference between the apparent contact angle and the equilibrium contact angle, while the viscous forces come from the inner fluid flow of the droplet and the contact line motion over the substrate. For larger θ_0, the more capillary force makes the spreading speed faster. When the contact angle is small, the effective spreading coefficient S_i has already been reduced to its equilibrium value $S_{eq}=\gamma_{LV}(\cos\theta_e-1)=0$. Therefore, the spreading rate tends to be exceedingly slow and stable.

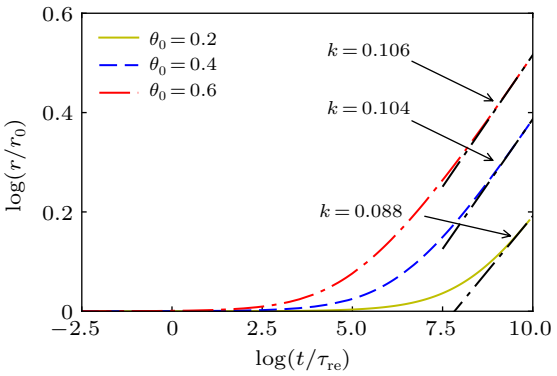


Fig. 2. Evolution of the contact line r/r_0 of drying droplets for three values of initial contact angles, $\theta_0=0.2$, 0.4, and 0.6. The time is in units of τ_{re}. The fitting tangent slopes k in the later evaporation processes confirm the Tanner's law. For all calculations, $\theta_e=0, k_{cl}=0$ and $k_{ev}=0$.

3. Result

In experiments, both frictionless and frictional substrates can be prepared by using different substrate materials and liquids. Various evaporation processes have been observed in experiments by changing the friction constant k_{cl} between the contact line and the substrates. The value of k_{cl} is determined by the substrate wetting properties, substrate defects, and surface-active solutes. We here simply take k_{cl} as a phenomenological parameter: k_{cl} is infinitely large for a pinned contact line, and is zero for a freely moving contact line. We discuss the drying of liquid droplets on both frictionless and frictional substrates, separately. This is inspired by previous experiments. Li *et al.*[6,7] experimentally showed that the CL of a water droplet can move freely on silica glass or polycarbonate substrate. This corresponds to the frictionless substrate case. On the other hand, they also showed that when water droplet is placed on a graphite substrate, the CL is almost pinned, representing a frictional substrate. We will focus on the droplet shape evolution during evaporation by analyzing the time evolution of the droplet contact line $r(t)$ and the droplet contact angle $\theta(t)$, which can be experimentally measured by using high-speed cameras. So all results are subject to experimental test.

3.1. Droplet on frictionless substrate

When the substrate is frictionless ($k_{\rm cl}=0$), the evolution equation of $\dot{R}(t)$ in Eq. (13) is reduced to

$$\dot{R}=-\frac{\gamma_{\rm LV}C_4(\theta)}{3\eta C_1(\theta)}. \tag{19}$$

Then we obtain the evolution equations of the contact line r from Eqs. (1), (2), and (19),

$$\begin{aligned}\tau_{\rm ev}\dot{\tilde{r}} =& -\frac{(1-\cos\theta_0)^2(2+\cos\theta_0)\cot\theta}{3\sin^3\theta_0\tilde{r}}\\ &+\frac{(1-\cos\theta)^2(\cos\theta_{\rm e}-\cos\theta)}{3C_1(\theta)k_{\rm ev}\sin\theta(1+\cos\theta)^2},\end{aligned} \tag{20}$$

and the contact angle evolution equation

$$\begin{aligned}\tau_{\rm ev}\dot{\theta} =& -\frac{(1-\cos\theta_0)^2(2+\cos\theta_0)}{3\sin^3\theta_0\tilde{r}^2}\\ &-\frac{(1-\cos\theta)^2(2+\cos\theta)(\cos\theta_{\rm e}-\cos\theta)}{3k_{\rm ev}C_1(\theta)(1+\cos\theta)^2\tilde{r}}.\end{aligned} \tag{21}$$

The two evolution equations seem to be complicated, however, they are just first-order differential equations that facilitate the numerical solutions. We will show that for some special case, the model can even give analytical results.

Figure 3 shows three typical droplet shape evolution processes for evaporation. When a droplet is placed on a substrate with an initial contact angle θ_0 and an equilibrium contact angle $\theta_{\rm e}$, it will perform three typical dynamics for $\theta_0<\theta_{\rm e}$, $\theta_0=\theta_{\rm e}$, and $\theta_0>\theta_{\rm e}$, respectively. The corresponding evolution of $r(t)$ and $\theta(t)$ is shown in Figs. 3(d) and 3(e), respectively. In order to have all these three dynamics, we assume a slow evaporation rate $k_{\rm ev}=0.001$, and set a fixed equilibrium contact angle, $\theta_{\rm e}=0.8$.

Figure 3(a) is the situation of $\theta_0<\theta_{\rm e}$, where we take $\theta_0=0.4$. The droplet contact line first shrinks quickly, meanwhile, its contact angle increases to $\theta_{\rm e}$. Then, r continuously decreases, while θ keeps constant due to the lose of volume. Figure 3(b) is for $\theta_0=\theta_{\rm e}=0.8$, which shows that r recedes homogeneously and θ keeps constant for most parts of the evaporation process. This is the CCA evaporation process observed in experiments[40]. On the other hand, when $\theta_0=1.2$, droplet first spreads to reduce the contact angle to its equilibrium value, and then recedes due to the lose of volume, as shown in Fig. 3(c).

It is clear that droplet shape evolution is determined by both the capillary effect and the evaporation effect. The capillary force arises from the difference between the apparent contact angle and the equilibrium value. When $\theta(t)$ is different from $\theta_{\rm e}$, droplet has to relax to its equilibrium contact angle. This is why r first recedes in Fig. 3(a), but first spreads in Fig. 3(c). Meanwhile, due to evaporation, the lose of volume tends to decrease r, explaining the later shrinking of the contact line in all situations. It is worth noting that when $k_{\rm cl}=0$, θ will be constant as long as it reaches its equilibrium value.

For this frictionless case, the contact angle evolution can also be changed by varying the evaporation rate. Figure 4 shows that when the evaporation rate is slow ($k_{\rm ev}=0.001$), the contact angle nearly stays unchanged for the whole evaporation process. However, it changes to a continuously decreasing mode for a fast evaporation rate ($k_{\rm ev}=1.0$) while all other parameters are the same.

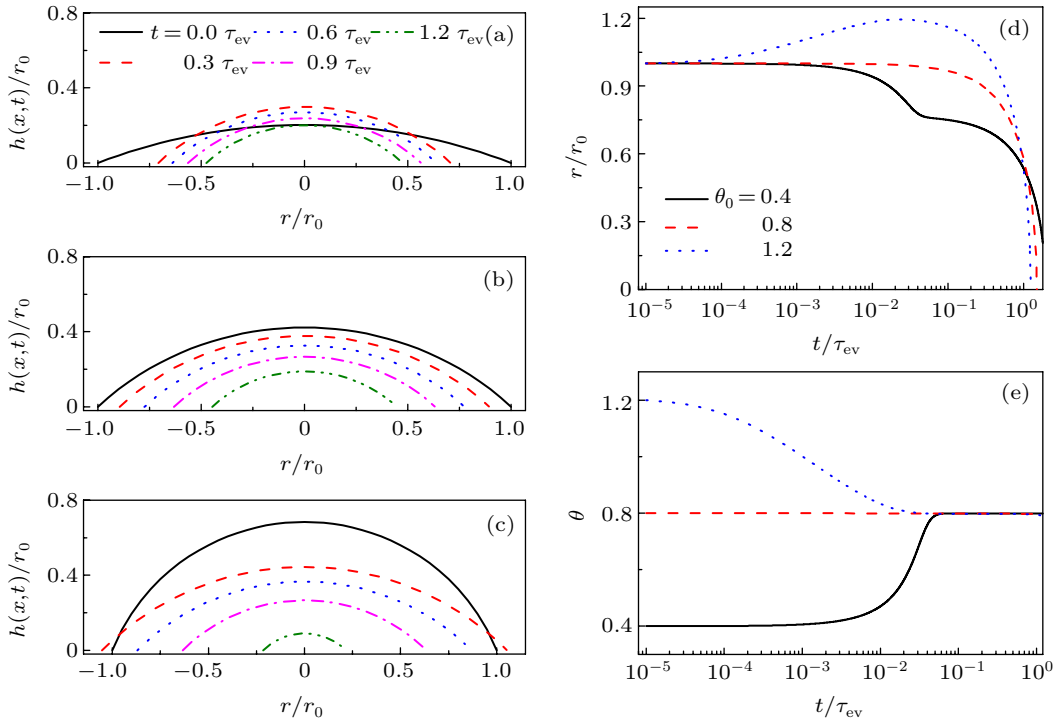


Fig. 3. Droplet shape evolution for evaporation on frictionless substrate for three situations: (a) $\theta_0<\theta_{\rm e}$, (b) $\theta_0=\theta_{\rm e}$, and (c) $\theta_0>\theta_{\rm e}$. The corresponding evolution of the contact line r/r_0 is shown in panel (d), and the contact angle θ is shown in panel (e). For all calculations, $\theta_{\rm e}=0.8$ and $k_{\rm ev}=0.001$.

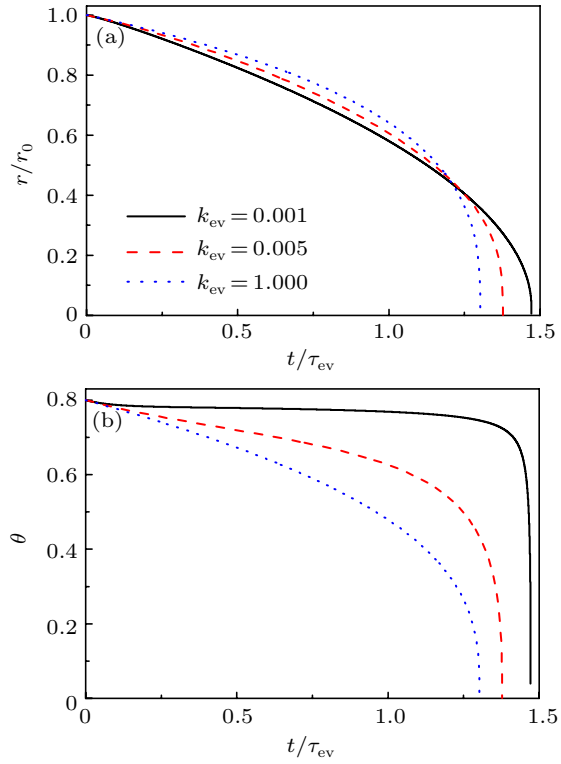


Fig. 4. Evolution of (a) contact radius r/r_0 and (b) contact angle θ of a drying droplet for various evaporation rates k_{ev}. By increasing the evaporation rate, the evolution mode changes from CCA to a continuously decreasing one. For all cases, the initial contact angle θ_0 of the droplet is the same as its equilibrium contact angle θ_e, and k_{cl} is fixed as $k_{cl}=0$.

An explicit expression of the droplet shape evolution equation can be obtained for the aforementioned CCA dynamics. For this case, we have an additional condition $\dot{\theta}=0$. Together with the empirical form of $\dot{V}$, we have the simple evolution equation of $r(t)$ as

$$\tilde{r}=\sqrt{1-\frac{2}{3}\tilde{t}}. \tag{22}$$

Figure 5 is the comparison of the results obtained by this simple model and the full Onsager model. The evolution of r is almost consistent between these two models, indicating that for this special case, such a simple model is enough to study the shape evolution of drying droplets. This may be useful for experimental quantitative comparisons.

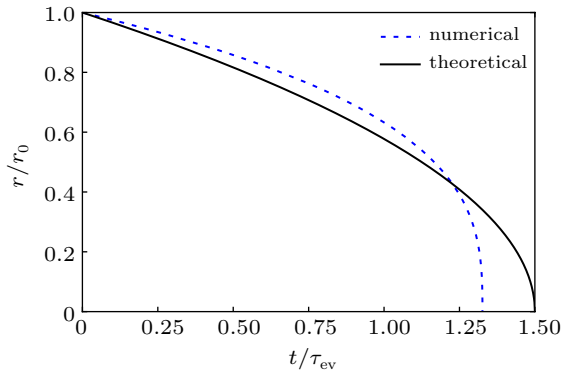


Fig. 5. The comparison of the evolution of r calculated from the simple model and the full Onsager model. The results are in good agreement. The parameters are: $\theta_0=\theta_e=0.4, k_{ev}=1, k_{cl}=0$.

3.2. Droplet on frictional substrate

When droplets evaporate on frictional substrate, the evaporation process becomes more complicated. For this case, besides the capillary and evaporation effects, a pinning force appears, which can also determine the motion of the droplet contact line.

From Eqs. (1), (2) and (13), we obtain the full evolution equation of r,

$$\begin{aligned}\tau_{ev}\dot{\tilde{r}}=&-\frac{(1-\cos\theta_0)^2(2+\cos\theta_0)\cos\theta}{3\sin^3\theta_0\sin\theta\tilde{r}}\\&+\frac{1-\cos\theta}{1+\cos\theta}\frac{\sin\theta}{3\sin\theta(1+\cos\theta)^2C_1(\theta)+k_{cl}(1-\cos\theta)^2}\\&\times\left[k_{cl}\frac{(1-\cos\theta_0)^2(2+\cos\theta_0)\cos\theta}{3\sin^3\theta_0\tilde{r}}+\frac{\sin\theta(\cos\theta_e-\cos\theta)}{k_{ev}}\right],\end{aligned} \tag{23}$$

and the contact angle evolution equation

$$\begin{aligned}\tau_{ev}\dot{\theta}=&-\frac{(1-\cos\theta_0)^2(2+\cos\theta_0)}{3\sin^3\theta_0\tilde{r}^2}\\&-\frac{(1-\cos\theta)^2(2+\cos\theta)}{3\sin\theta(1+\cos\theta)^2C_1(\theta)+k_{cl}(1-\cos\theta)^2}\\&\times\left[k_{cl}\frac{(1-\cos\theta_0)^2(2+\cos\theta_0)\cos\theta}{3\sin^3\theta_0\tilde{r}^2}+\frac{\sin\theta(\cos\theta_e-\cos\theta)}{k_{ev}\tilde{r}}\right].\end{aligned} \tag{24}$$

We want to emphasize that the full model is reduced to the evolution equations (20) and (21) by taking $k_{cl}=0$.

We have shown the freely moving cases in the previous subsection. We here analyze the droplet shape evolution for both small $k_{cl}=25$ and large $k_{cl}=1000$, separately.

Figure 6(a) is for droplet evaporating on substrate with $k_{cl}=1000$, an equilibrium contact angle $\theta_e=0.2$, an initial contact angle $\theta_0=0.8$, and the evaporation rate $k_{ev}=0.01$. Although $\theta_0\neq\theta_e$, the strong pinning force makes the contact line r nearly unchanged during most parts of the evaporation process, as shown in Fig. 6(b) (the black solid line). Meanwhile, the contact angle keeps decreasing due to the lose of volume, indicating by the blue dashed line in Fig. 6(b). For a small value of $k_{cl}=25$ in Figs. 6(c) and 6(d), r is first pinned, and then starts to recede. The first pinned of the contact line is because of the pinning force. The later receding is mainly due to the increase of the evaporation rate, as we assume that $J(t)$ is an inverse function of r.

When the contact line is nearly pinned during most parts of the evaporation process, it is named as CCR process observed in experiments. For this special case, $\dot{r}=0$ and together with the form of $\dot{V}$ leading to a simple evolution equation of θ,

$$\dot{\theta}=-\frac{(1-\cos\theta_0)(2+\cos\theta_0)}{3\tau_{ev}\sin\theta_0(1+\cos\theta_0)}(1+\cos\theta)^2. \tag{25}$$

This equation clearly shows that θ keeps decreasing because $\dot{\theta}<0$.

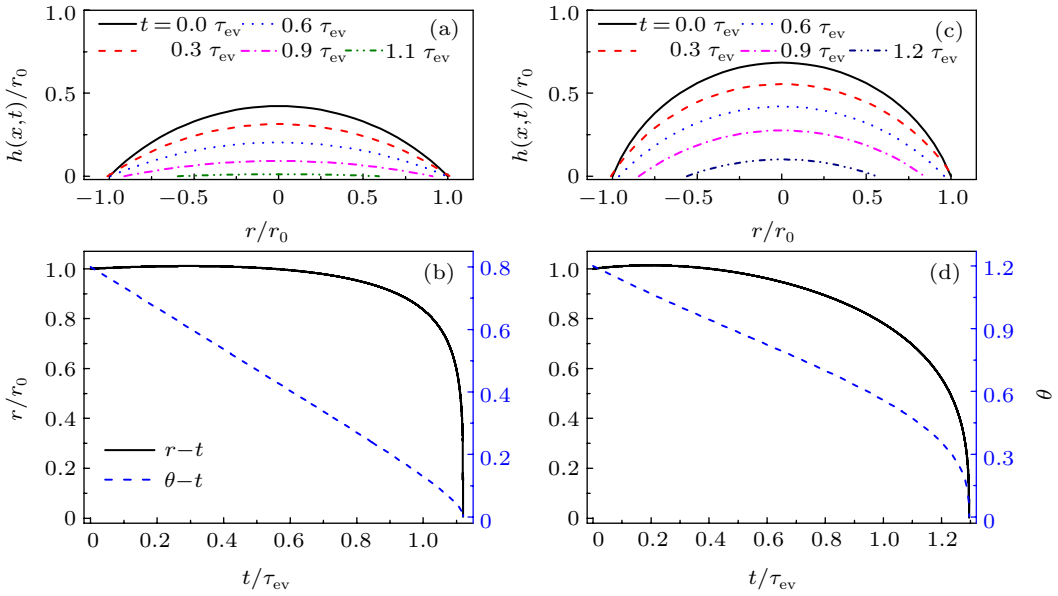


Fig. 6. Droplet shape evolution on frictional substrate. Panel (a) is for pinned contact line motion with $k_{cl} = 1000$. Panel (b) is the corresponding evolution of r/r_0 and θ. Panel (c) is the shape evolution for small $k_{cl} = 25$, and its corresponding evolution of r/r_0 and θ is shown in panel (d). The calculation parameters for panels (a) and (b) are $\theta_0 = 0.8$, $\theta_e = 0.2$, and $k_{ev} = 0.01$, while for panels (c) and (d), $\theta_0 = 1.2$, $\theta_e = 0.6$, and $k_{ev} = 0.5$.

Figure 7 is the comparison of the results obtained by this simple model and the full Onsager model. The evolution of θ is almost consistent between these two models, indicating that for this special case, such a simple model is enough to study the shape evolution of drying droplets.

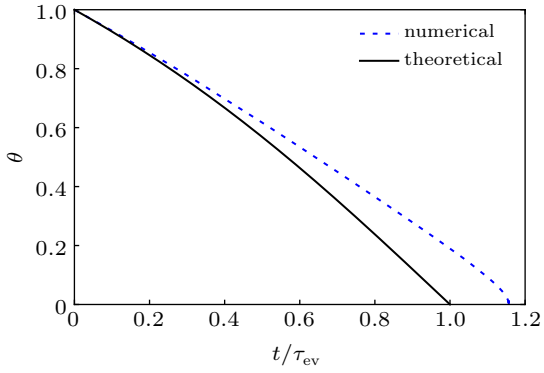


Fig. 7. The comparison of θ evolution between the reduced model and the Onsager full model when the contact line is pinned, $\dot{r} = 0$. The calculation parameters are: $\theta_0 = 1.0, \theta_e = 0, k_{ev} = 1, k_{cl} = 1000$.

4. Discussion and conclusion

In this article, we have proposed a simple model for the shape evolution of drying droplets. We assume a spherical shape of the droplet liquid/vapor interface, enabling the study of drying droplets on both hydrophobic and hydrophilic substrates. The model provides a generally quantitative study of the effects of the friction between the CL and the substrate, the capillary force and the evaporation rate in the droplet evaporation dynamics. The friction of the CL/substrate causes two motions of the CL, i.e., pinned or depinned. The capillary force, arising from the difference between the apparent contact angle and the equilibrium contact angle, leads to the spreading or receding motion of the CL. The evaporation tends to cause the receding motion of the CL due to the lose of volume. One realistic evaporation process is determined by the combined effects of the three factors, resulting in various droplet shape evolution processes.

When the substrate is frictionless ($k_{cl} = 0$), the CL can move freely over the substrate. In this case, the capillary force and the evaporation rate dominate the droplet evaporation process. On the other hand, when it is frictional substrate ($k_{cl} \neq 0$), k_{cl} is an additional factor to determine the droplet shape evolution. When the evaporation rate is slow, the model demonstrates two experimentally observed evaporation processes: the CCA by taking $k_{cl} = 0$, and the CCR by setting a large value of k_{cl}. Moreover, complicated evaporation processes are also obtained, for example, the contact radius first spreads and then shrinks when the initial contact angle is larger than the equilibrium contact angle.

In addition to the full Onsager model, we have also proposed three analytical models for some special cases. When $k_{cl} = 0$ and there is no evaporation, the Onsager model reduces to the famous Tanner's law, giving a scaling law of r as a function of time t, $r \sim t^{\frac{1}{10}}$. Analytical evolution equations of both $\dot{r}$ and $\dot{\theta}$ are also given corresponding to experimental situations of the CCA and the CCR processes, respectively. These simple expressions are not only consistent with full Onsager model calculations, but also provide a quantitative comparison between experimental measurements and theoretical studies, facilitating the understanding of the physical mechanism underlying the drying of liquid droplets.

Since there are various parameters determining the evaporation of droplets in experiments, it is difficult to make a quantitative comparison between the theory and experiments.

However, a qualitative comparison of the evaporation modes can be made. In experiment and simulation studies, for the evaporation of droplets on weak contact angle hysteresis substrates, the contact line of droplet can move freely on the substrate and the droplet evaporates in the CCA mode.[14–16,19–21] This is consistent with the present theoretical results by setting k_{cl} to 0 or very small values. While on strong contact angle hysteresis substrates, the pinning force of the contact line is very large and the droplets evaporate in the CCR mode or mixed mode.[14,18–21] This is related to the theory by setting k_{cl} to large values. On the other hand, experiments also show that decreasing the surrounding saturated vapor pressure,[15] the evaporation mode of droplet changes from CCA to mixed mode, which is also in agreement with our theory by increasing the evaporation parameter k_{ev} as shown in Fig. 4.

In terms of the evaporation rate, we notice that it is also affected by the heterogeneous distribution of temperature and the physical-chemical properties of the substrate.[41,42] We here assume a homogeneous evaporation rate that is a function of the droplet radius during evaporation. However, when one wants to study more complicated droplet evaporation, all these extra effects must be included in the model in the future.

The simple Onsager variational principle model of drying droplets is for droplets with a single component, but can be extended to mixed liquid droplets. Although we only focus on the droplet shape evolution in this article, the corresponding deposition patterns can also be obtained for droplets placed on both hydrophobic and hydrophilic substrates. The Onsager model can also be applied to the study of droplet motion by assuming that the position of the droplet center can be moved.

References

[1] Deegan R D 2000 *Phys. Rev. E* **61** 475
[2] Bonn D, Eggers J, Indekeu J, Meunier J and Rolley E 2009 *Rev. Mod. Phys.* **81** 739
[3] Deegan R D, Bakajin O, Dupont T F, Huber G, Nagel S R and Witten T A 1997 *Nature* **389** 827
[4] Marín Á G, Gelderblom H, Lohse D and Snoeijer J H 2011 *Phys. Rev. Lett.* **107** 085502
[5] Willmer D, Baldwin K A, Kwartnik C and Fairhurst D J 2010 *Phys. Chem. Chem. Phys.* **12** 3998
[6] Li Y F, Sheng Y J and Tsao H K 2013 *Langmuir* **29** 7802
[7] Li Y F, Sheng Y J and Tsao H K 2014 *Langmuir* **30** 7716
[8] Kajiya T, Monteux C, Narita T, Lequeux F and Doi M 2009 *Langmuir* **25** 6934
[9] Fukuda K, Sekine T, Kumaki D and Tokito S 2013 *ACS Appl. Mater. Interfaces* **5** 3916
[10] Wu M M, Man X K and Doi M 2018 *Langmuir* **34** 9572
[11] Shrikanth V, Archana S and Bobji M S 2019 *Meas. Sci. Technol.* **30** 075002
[12] Yu Y, Zhu H, Frantz J M, Reding M E, Chan K C, Ozkan H E 2009 *Biosyst. Eng.* **104** 324
[13] Li H Y, Tee B C-K, Cha J J, Cui Y, Chung J W, Lee S Y and Bao Z N 2012 *J. Am. Chem. Soc.* **134** 2760
[14] Picknett R G and Bexon R 1977 *J. Colloid Interface Sci.* **61** 336
[15] Bourg'es-Monnier C B and Shanahan M E R 1995 *Langmuir* **11** 2820
[16] Erbil H Y, McHale G and Newton M I 2002 *Langmuir* **18** 2636
[17] Kim J H, Ahn S I and Zin W C 2007 *Langmuir* **23** 6163
[18] Shrikanth V, Archana S and Bobji M S 2019 *Meas. Sci. Technol.* **30** 075002
[19] Wang F C and Wu H A 2013 *Soft Matter* **9** 5703
[20] Liu Y and Zhang X 2013 *Phys. Rev. E* **88** 012404
[21] Sun Y J, Huang T, Zhao J F, Chen Y 2017 *Front. Phys.* **12** 126401
[22] Deegan R D, Bakajin O, Dupont T F, Huber G, Nagel S R and Witten T A 2000 *Phys. Rev. E* **62** 756
[23] Hu H and Larson R G 2002 *J. Phys. Chem. B* **106** 1334
[24] Hu H and Larson R G 2005 *Langmuir* **21** 3963
[25] Freed-Brown J 2014 *Soft Matter* **10** 9506
[26] Mouat A P, Wood C E, Pye J E and Burton J C 2020 *Phys. Rev. Lett.* **124** 064502
[27] Frastia L, Archer A J and Thiele U 2011 *Phys. Rev. Lett.* **106** 077801
[28] Thampi S P, Pagonabarraga I, Adhikaric R and Govindarajan R 2016 *Soft Matter* **12** 6073
[29] Doi M 2011 *J. Phys.: Condens. Matter* **23** 284118
[30] Doi M 2013 *Soft Matter Physics* (New York: Oxford University Press) pp. 114–135
[31] Doi M 2015 *Chin. Phys. B* **24** 020505
[32] Onsager L 1931 *Phys. Rev.* **37** 405
[33] Onsager L 1931 *Phys. Rev.* **38** 2265
[34] Onuki A 2002 *Phase Transition Dynamics* (Cambridge: Cambridge University Press)
[35] Doi M 2009 *J. Phys. Soc. Jpn.* **78** 052001
[36] Parisse F and Allain C 1997 *Langmuir* **13** 3598
[37] Kobayashi M, Makino M, Okuzono T and Doi M 2010 *J. Phys. Soc. Jpn.* **79** 044802
[38] Snoeijer J H and Andreotti B 2013 *Annu. Rev. Fluid Mech.* **45** 269
[39] Ding H and Spelt P D M 2007 *J. Fluid Mech* **576** 287
[40] Erbil H Y, McHale G and Newton M I 2002 *Langmuir* **18** 2636
[41] Pan Z H, Dash S, Weibel J A, and Garimella S V 2013 *Langmuir* **29** 15831
[42] Duan F, He B, and Wei T 2015 *J. Nanosci. Nanotechnol.* **15** 3011